



HAL
open science

STEM-EELS identification of TiOXNY, TiN, Ti₂N and O, N dissolution in the Ti₂₆₄₂S alloy oxidized in synthetic air at 650 °C

Iman Abdallah, Charlotte Dupressoire, Lydia Laffont, Daniel Monceau,
Aurélie Vande Put

► To cite this version:

Iman Abdallah, Charlotte Dupressoire, Lydia Laffont, Daniel Monceau, Aurélie Vande Put. STEM-EELS identification of TiOXNY, TiN, Ti₂N and O, N dissolution in the Ti₂₆₄₂S alloy oxidized in synthetic air at 650 °C. Corrosion Science, 2019, 153, pp.191-199. 10.1016/j.corsci.2019.03.037 . hal-02115253

HAL Id: hal-02115253

<https://hal.science/hal-02115253>

Submitted on 30 Apr 2019

HAL is a multi-disciplinary open access archive for the deposit and dissemination of scientific research documents, whether they are published or not. The documents may come from teaching and research institutions in France or abroad, or from public or private research centers.

L'archive ouverte pluridisciplinaire **HAL**, est destinée au dépôt et à la diffusion de documents scientifiques de niveau recherche, publiés ou non, émanant des établissements d'enseignement et de recherche français ou étrangers, des laboratoires publics ou privés.



Open Archive Toulouse Archive Ouverte (OATAO)

OATAO is an open access repository that collects the work of Toulouse researchers and makes it freely available over the web where possible

This is an author's version published in: <http://oatao.univ-toulouse.fr/23796>

Official URL: <https://doi.org/10.1016/j.corsci.2019.03.037>

To cite this version:

Abdallah, Iman  and Dupressoire, Charlotte  and Laffont, Lydia  and Monceau, Daniel  and Vande Put, Aurélie  *STEM-EELS identification of TiOXNY, TiN, Ti2N and O, N dissolution in the Ti2642S alloy oxidized in synthetic air at 650 °C.* (2019) Corrosion Science, 153. 191-199. ISSN 0010-938X

Any correspondence concerning this service should be sent to the repository administrator: tech-oatao@listes-diff.inp-toulouse.fr

STEM-EELS identification of TiO_xN_y , TiN , Ti_2N and O, N dissolution in the Ti6242S alloy oxidized in synthetic air at 650 °C

Iman Abdallah*, Charlotte Dupressoire, Lydia Laffont, Daniel Monceau, Aurelie Vande Put

CIRIMAT, Université de Toulouse, CNRS, INP-ENSIACET, 4 allée Emile Monso, BP 44362, 31030, Toulouse Cedex 4, France

ARTICLE INFO

Keywords:

A. Titanium
A. Alloys
B. STEM
C. Interfaces
C. Oxidation

ABSTRACT

Oxide-alloy interface of Ti6242S Ti-based alloy was investigated by STEM-EELS technique, after oxidation in both N_2 -free and synthetic air atmospheres at 650 °C for 1000 h. The chemical shift of $\text{Ti-L}_{2,3}$ edge and its specific fine structure along the oxide-alloy interface were used as fingerprint to distinguish the different compositions of titanium nitrides and oxynitrides. TiN , Ti_2N and TiN_xO_y were identified in the sample oxidized in synthetic air at the oxide-alloy interface. Moreover, a decreasing in the oxidation state of Ti oxides was found along with Sn segregation at the oxide-alloy interface for the sample oxidized in N_2 -free atmosphere.

1. Introduction

Titanium-based alloys such as $\text{Ti6Al2Sn4Zr2Mo0.1Si}$ (Ti6242S) are widely used in the aerospace industry because of their high specific mechanical strength. However, at high temperatures and under oxidizing conditions, Ti-based alloys undergo oxygen dissolution in addition to the growth of an oxide scale. Depending on time and duration, the oxygen dissolution can affect large depths, which can greatly alter mechanical properties [1,2]. Nitrogen, main air constituent, can also dissolve in titanium and its alloys [3]. In 1986, Chaze and Coddet early reported the decrease in oxidation kinetics of titanium and Ti-X alloys (with $X = \text{Al}$, Cr or Si) when oxidized in a nitrogen-rich environment [4]. They set out three hypotheses to explain such nitrogen effect: (i) decrease in oxygen vacancy concentration in the rutile, (ii) decrease in oxygen solubility within the metallic alloy, (iii) nitride formation at the oxide-alloy interface. However, they did not show any experimental data proving any of these hypotheses. Three recent works brought experimental evidences on the nitrogen effect on the oxidation behavior along the oxide-alloy interface [5–7]. Kanjer et al. reported the formation of a continuous nitrogen-rich layer observed by nuclear reaction analysis between the oxide layer and shot-peened grade I titanium, after oxidation at 700 °C for 100 h in dry air [5]. Dupressoire et al. compared the oxidation behavior of Ti6242S Ti-based alloy at 650 °C in synthetic air (80% N_2 - 20% O_2) and under 80% Ar - 20% O_2 for 100 [6] and 1000 h [7]. Whatever the duration, they observed a decrease in mass variation as well as a decrease in dissolved oxygen and oxygen concentration at the oxide-alloy interface when the alloy was exposed to the nitrogen-rich environment. Micro-tips were then prepared from

Ti6242S samples exposed to both atmospheres and atom probe tomography (APT) was performed [7]. While TiO was noticed above the α -Ti phase containing up to 24.5 at. % of oxygen in the tip related to the oxidation in 80% Ar - 20% O_2 , concentration profiles close to Ti_2N and an oxynitride were noticed in the tip associated to the synthetic air exposure, above a metallic phase containing only 0.8 at. % of oxygen. To confirm this, the oxide-alloy interface of Ti6242S alloy exposed in the same conditions (1000 h at 650 °C under synthetic air or 80% Ar -20% O_2) was characterized by electron energy loss spectroscopy (EELS) technique.

The EELS technique allows obtaining local information at a nanometer scale and quantifying the element contents and phase evolution at an atomic level across the interface. Besides, based on the fine structure, the energy threshold and the shift of the $\text{Ti-L}_{2,3}$ edges could differentiate the chemical composition and its crystallographic structure such as TiN , Ti_2N and metallic α -Ti [8–10].

2. Experimental techniques

2.1. Materials

Ti6242S alloy studied in this work was forged by Aubert & Duval (Pamiers, France) and presented a duplex microstructure. Its chemical composition, determined by energy dispersive X-ray spectroscopy (EDX), was 10.5 Al, 2.1 Zr, 1.0 Mo, 0.7 Sn, 0.2 Si in at. %. Its composition in gas forming elements, measured by instrumental gas analyses by Evans Analytical Group (Tournefeuille, France) was 3550 O, 2062 H, 103 C, 12 S and < 17 N in at. % ppm. $15 \times 10 \times 1 \text{ mm}^3$ samples were

* Corresponding author.

E-mail address: iman.abdallah@ensiacet.fr (I. Abdallah).

ground using P240 SiC paper and then cleaned in acetone and ethanol in ultrasound baths before oxidation under synthetic air and 80% Ar-20% O₂ for 1000 h at 650 °C. More details on the oxidation tests can be found in [6,7].

2.2. Characterization

Three cross-sectional 10 × 10 μm² samples were prepared using a focused-ion beam (FIB) FEI HELIOS 600i apparatus. Two samples were made from two regions, so called Region I and Region II, randomly chosen from the surface of the Ti6242S specimen oxidized for 1000 h in synthetic air while only one sample was obtained from the same alloy oxidized for 1000 h under 80% Ar-20% O₂. These samples were studied and chemically analyzed using a JEOL cold-FEG JEM-ARM 200 F transmission electron microscope (TEM), operated at 200 kV and equipped with a Cs corrector probe of 0.078 nm spatial resolution. Characterizations were done using the high-angle annular dark field (HAADF) scanning TEM (STEM) mode. Energy dispersive X-ray (EDX) and electron energy loss spectroscopy (EELS) techniques were used to identify the oxygen and nitrogen content evolution across the oxide-alloy interface. EDX qualitative maps and line scans of the sample were acquired with a JEOL CENTURIO SDD detector. EELS spectra were recorded using a GIF Quantum ER imaging filter. Collective and convergence semi angles were 19.4 and 14.8 mrad respectively. The energy resolution of 0.5 eV was determined using the full width half maximum (FWHM) of the recorded zero-loss peak. EELS line scans were recorded from the oxide scale towards the alloy passing through the oxide-alloy interface. An energy dispersion of 0.1 eV/channel was chosen to acquire the Ti-L_{2,3}, N-K and O-K energy loss near edge spectra (ELNES). Each spectrum was acquired every 0.5 nm to monitor the evolution of the chemical shift and the fine structure changes in the Ti-L_{2,3} edge profile.

3. Results and discussion

3.1. Ti6242S sample oxidized in synthetic air: (Region I)

Fig. 1a presents a low magnification STEM-HAADF image showing the oxide layer, the oxide-alloy interface and the Ti6242S alloy. STEM-HAADF image contrast depends on the atomic number (Z), such that the brighter and darker regions correspond to higher and lower Z respectively. The oxide scale formed in synthetic air was 2 ± 0.1 μm thick and exhibited porosity in its upper part and close to the oxide-alloy interface. Several researchers also reported the formation of a porous oxide

scale on Ti6242S after a change in oxidation behavior from parabolic to linear above 700 °C [11,12]. Stratification of the oxide layer near the oxide-alloy interface is also observed. This phenomenon is mostly explained by the development of compressive stresses within the oxide and tensile stresses in the alloy, due to the high value of the Ti/TiO₂ Pilling and Bedworth ratio. When the stresses at the oxide-alloy interface reach a bearable maximum value, corresponding to a critical TiO₂ thickness, cracking at the oxide-alloy occurs [13–15].

Rutile TiO₂ (space group: P4₂/mmm, lattice parameters: a = 4.5933 Å and c = 2.9592 Å from JCPDS no. 00-021-1276) was identified within the oxide scale, as highlighted by the selected area electron diffraction (SAED) pattern in Fig. 1a taken from an aperture of 300 nm size denoted by the small circle in the oxide layer. This is consistent with our previous study where rutile TiO₂ was detected by X-ray diffraction and Raman spectroscopy in addition to α-alumina identified by fluorescence spectroscopy [6]. In the Ti6242S alloy, the β-phase (white contrast in Fig. 1a) was easily visible within the α-matrix. Among the alloying elements, Al and O are α-stabilizers and Mo is β-stabilizer, Zr and Si being neutral elements. Qualitative EDX maps of the whole area are presented in Fig. 1b; where four chemical elements are highlighted as: Ti-K_α, Al-K_α, O-K_α and Mo-L_α. It confirms that Mo partitions preferentially form in the β-phase.

Two regions of Fig. 1a were selected to check their chemical compositions: 1- red square in the upper oxide layer and 2- green square at the oxide-alloy interface. Fig. 2 presents the zoom of the STEM-HAADF image on the upper oxide layer and its corresponding EDX maps where Ti-K_α, Al-K_α, O-K_α were selected. Al-rich oxides were detected on top of the TiO₂ layer, which was confirmed by EDX and coherent with our previous work [6]. Its presence in the upper part of the oxide layer is also in agreement with a study of Chaze and Coddet [16] on the effect of aluminum on the oxidation behavior of titanium between 550 and 750 °C. The presence of an alumina layer, which is a very stable oxide, at the external surface of the TiO₂ scale has been observed on different alloys which form a rutile oxide scale: Ti₃Al [17], TA6V [18], Ti-46Al-8Nb [19]. This phenomenon was explained by relative diffusion kinetics, *i.e.* kinetic demixing. Indeed, it is known that Al diffuses very fast along channels in the c-axis of the rutile crystal, therefore this specie segregates at the external part of the scale (see [17]). Passing through the oxide-alloy interface as shown in Fig. 3, a particular attention was made on the nitrogen content in the EDX maps. It is noticeable the Al, Ti and O are present in the oxide layer just before the interface, whereas nitrogen is ambiguously present in the alloy next to the interface. To verify the nitrogen content, EDX acquisitions were

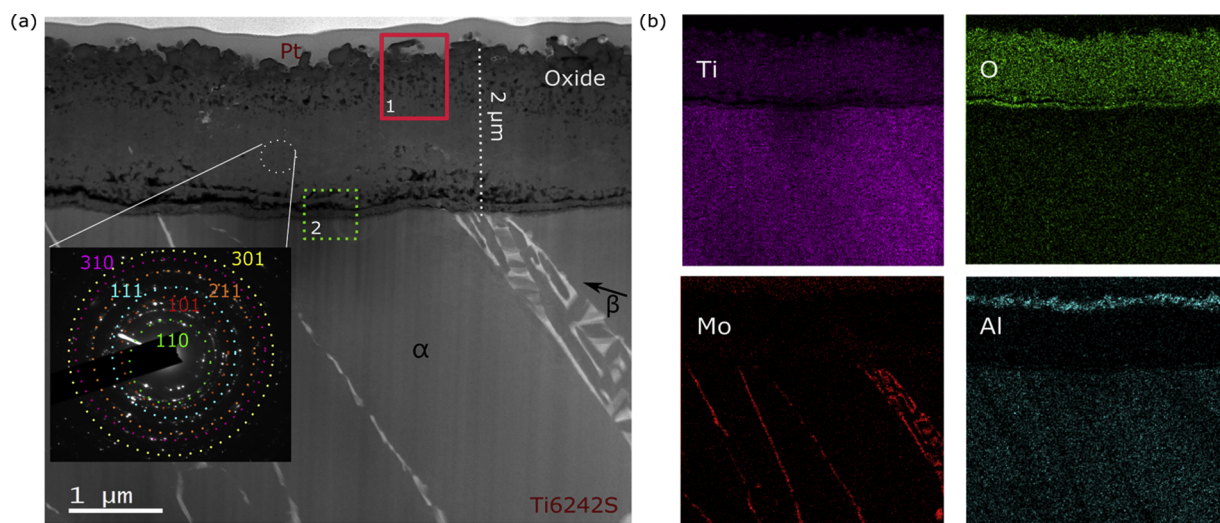


Fig. 1. (a) STEM-HAADF image of region (I) of the Ti6242S sample oxidized in synthetic air at 650 °C for 1000 h with an inset of selected area electron diffraction pattern of the oxide layer obtained from a 300 nm aperture. (b) Qualitative EDX maps of the whole area showing Ti, Mo, Al and O chemical elements. (For interpretation of the references to colour in the text, the reader is referred to the web version of this article.)

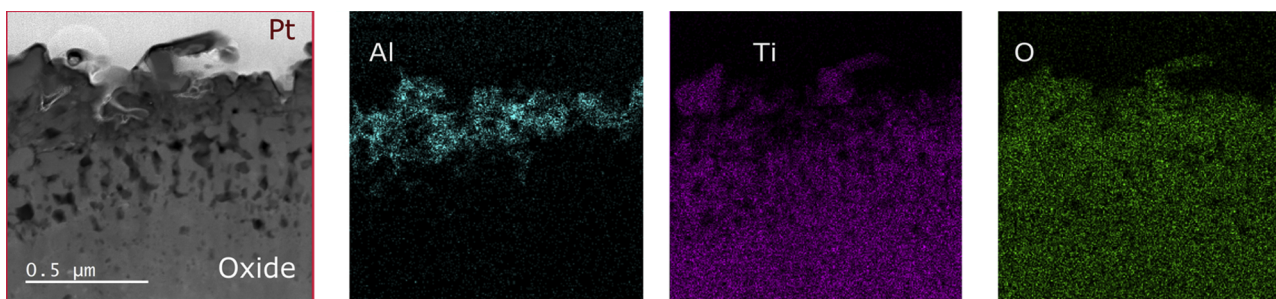


Fig. 2. STEM-HAADF image on the upper part of the oxide layer with its corresponding EDX qualitative maps of region (I) of Ti6242S oxidized at 650 °C for 1000 h in synthetic air.

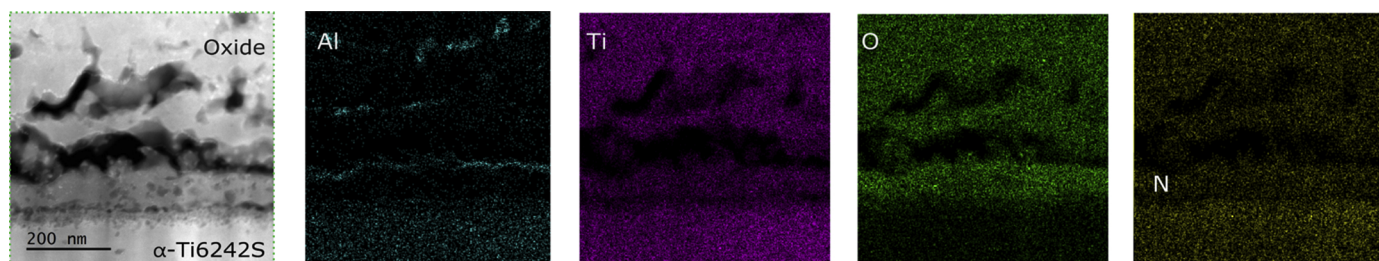


Fig. 3. STEM-HAADF image on the oxide-alloy interface with its corresponding EDX qualitative map of region (I) of the Ti6242S oxidized at 650 °C for 1000 h in synthetic air.

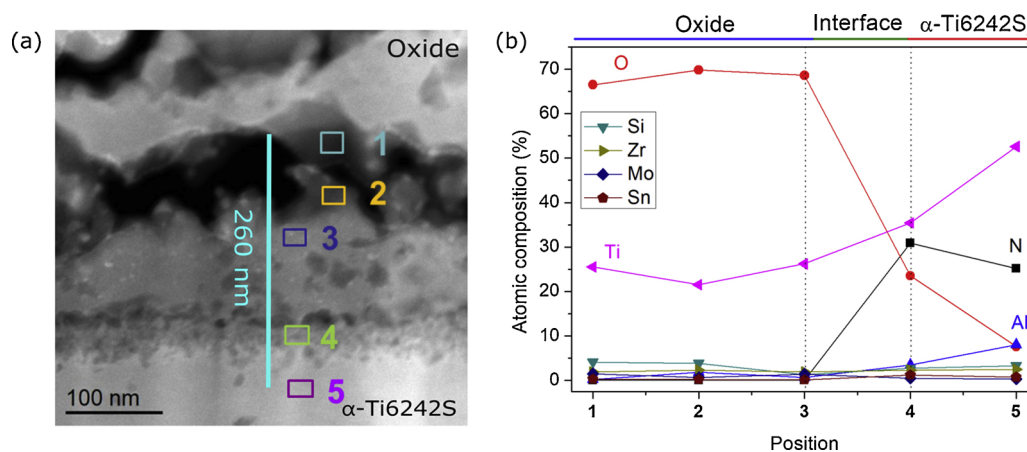


Fig. 4. STEM-HAADF image of region (I) of Ti6242S oxidized at 650 °C for 1000 h in synthetic air at (a) the oxide-alloy interface and (b) corresponding atomic compositions of 5 EDX selected areas positions.

done on selected areas on the same STEM image of Fig. 3. The selected areas were chosen to be large enough so the intensity counts are sufficient to quantify the composition of the constituent element (Fig. 4). The selected areas taken at positions 1, 2 and 3 indicate a Ti-rich oxide phase in the oxide layer, whereas the other elements have a composition less than 4 at. %. At position 4, the selected area is taken at the oxide-alloy interface and monitors an abrupt increase in the nitrogen content and a decrease in the oxygen content respectively. After the oxide layer, in the α -phase of Ti6242S, at position 5, the decrease in oxygen content is clear along with the decrease in nitrogen. It is noticeable also that Ti and Al contents increase which indicates the α -Ti phase.

In general, EDX technique presents a qualitative information of almost all contained elements of the periodic table with detection limitations for light elements. EELS technique offers much more sensitivity compared to EDX for light element detection such as nitrogen and oxygen. For this, EELS line scan probe passing from the oxide scale towards the alloy was acquired in a 0.5 nm step size to identify the phases present at the oxide-alloy interface and their compositions.

Transition metals (such as Ti) ELNES spectra are identified by the white L_3 and L_2 lines due to spin-orbit splitting of 2p core hole and transition to 3d states [20,21]. The L_3 ($2p_{3/2} \rightarrow 3d$) and L_2 ($2p_{1/2} \rightarrow 3d$) white lines of metallic Ti are usually detected at 457 and 462.5 eV respectively [8]. In all of the following EELS treatment, the background prior to the edges was fitted by a power law method and subtracted off so that only the Ti- $L_{2,3}$, N-K and O-K edges are shown. Fig. 5a presents a STEM-HAADF image of the oxide-alloy interface. The latter is composed of four regions: (i) oxide (40 ± 2 nm), (ii) interface (13 ± 2 nm), (iii) nitride (30 ± 2 nm) and (iv) Ti6242S alloy. By APT, a nitrogen, oxygen and titanium rich phase was detected over few nanometers on the very end of one micro-tip at the oxide-alloy interface [7]. On this same micro-tip, an oxygen concentration of 4 at. % and 0.8 at. % was measured within Ti_2N (~ 20 nm thick) and the α -phase below the oxynitride region respectively [7]. Fig. 5b presents all the EELS spectra of Ti- $L_{2,3}$, O-K and N-K edges where the modification of the fine structure of the Ti- $L_{2,3}$ along the line scan and the energy shift of the three edges for the four regions from oxide to Ti6242S can be seen. In this study, *i.e.* using the EELS technique, it is interesting to note the absence of N-K

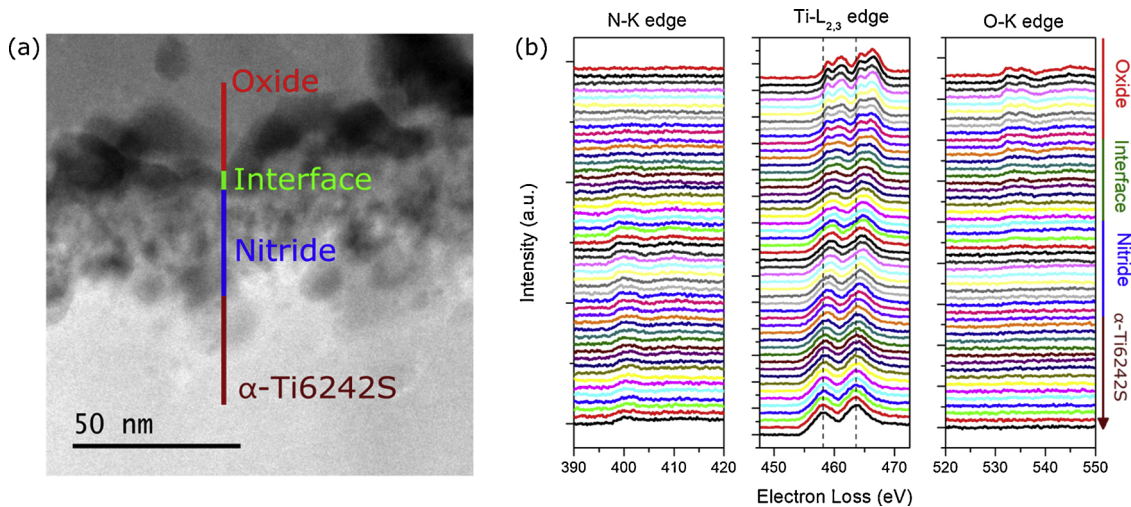


Fig. 5. STEM-HAADF image of region (I) of Ti6242S oxidized at 650 °C for 1000 h in synthetic air at (a) the oxide-alloy interface and (b) its corresponding ELNES spectra of N-K, Ti- $L_{2,3}$ and O-K edges acquired along the line drawn on (a).

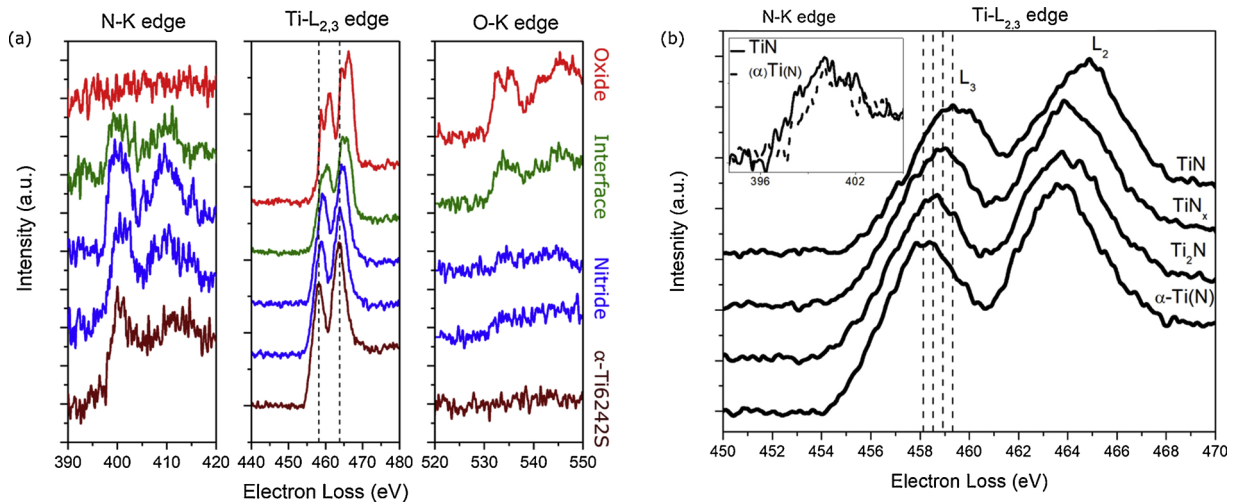


Fig. 6. A zoom on ELNES N-K, Ti- $L_{2,3}$ and O-K spectra showing the fine structure changes and the chemical shift of these edges for each region through the oxide-alloy interface in (a) and (b) the evolution of Ti- $L_{2,3}$ spectra passing from TiN to Ti_2N and Ti(N) in the nitride region with an inset of N-K edge comparison between TiN and Ti(N). (For interpretation of the references to colour in the text, the reader is referred to the web version of this article.)

edge in the oxide region as well as the absence of O-K edge in the titanium nitride and Ti6242S region.

To follow the variation of the fine structure from the acquired EELS spectra, one N-K, Ti- $L_{2,3}$ and O-K ELNES spectrum of each region is plotted in Fig. 6a indicated by red, green, blue and brown. The core loss spectra of N-K, O-K and Ti- $L_{2,3}$ provide local information about the chemical bonding around the excited atoms. Thus, changes in the fine structure or an energy shift is an indication of different chemical compositions and/or crystallographic structure modifications. The oxide layer shows Ti- $L_{2,3}$ and O-K edge ELNES spectra with the absence of N-K edge. Besides, the Ti- $L_{2,3}$ and O-K edges were compared with those of reference samples of rutile and anatase where the asymmetry of the peaks and threshold energy position is a direct indication of the crystalline structure [19,22–25]. Brydson et al. and Ruus et al. showed that this asymmetry is resolved into two peaks by high resolution X-ray absorption (XAS) [23,26]. As also seen by electron diffraction, the presence of TiO₂ rutile is confirmed by the fingerprint approach of the fine structure. The oxidation state of rutile TiO₂ is shown by the split of Ti- L_2 and L_3 white lines into 4 peaks as shown in Fig. 6a. In rutile (or anatase) structure, the octahedral coordination of Ti atoms with oxygen splits the degeneracy of unoccupied 3d states (each white line) into lower t_{2g} and higher e_g bands [27]. At the interface, the O-K edge

intensity decreases and its profile changes along with the appearance of the N-K edge, highlighting the presence of a titanium oxynitride and confirming the APT observations. It is also noticeable that the white lines L_3 and L_2 of Ti have changed. A shift to a lower energy loss value is also detected. For this, the modifications of Ti- L_3 and L_2 fine structure (four to two peaks) are due to changes in the atomic structure of the first atomic shells around the absorbed atoms. After the oxynitrides of titanium and as nitrogen occupies all the anionic vacancies, the N-K edge peak increased in intensity indicating the nitrogen concentration was greater in the nitride region with the absence of oxygen O-K edge. Oxygen/nitrogen vacancies, defects and changes in lattice parameter from TiO₂ tetragonal rutile to cubic rock salt TiN_x structure (x changes as a function of the chemical shift observed in Fig. 6b) affected the electron energy loss intensity and led to a shift to lower energy values.

To identify the formed titanium nitride, Ti- $L_{2,3}$ and N-K edges were compared with the study of Terada et al. on the chemical shift of Ti- L_3 edge at TiN/Ti interface [8]. They attributed this shift to a change in the chemical bonding of Ti with nitrogen atoms where a certain amount of charge transfers from Ti to N. Experimental ELNES were also verified with simulation using calculated band structure by Khin et al. and Terada et al. [8–10]. In [8], experimental ELNES spectra were compared with calculated Ti- L_3 ELNES depending on the nitrogen vacancies

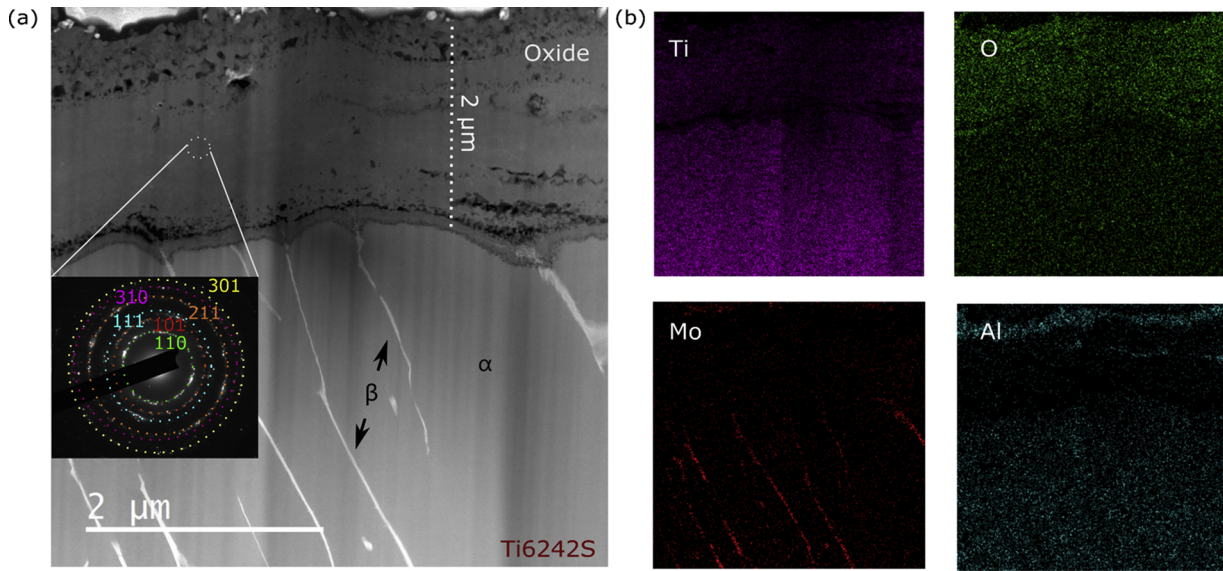


Fig. 7. (a) STEM-HAADF image of region (II) of the Ti6242S sample oxidized in synthetic air at 650 °C for 1000 h with an inset of selected area electron diffraction pattern of the oxide layer obtained from a 300 nm aperture. (b) Qualitative EDX maps of the whole area showing Ti, Mo, Al and O chemical elements.

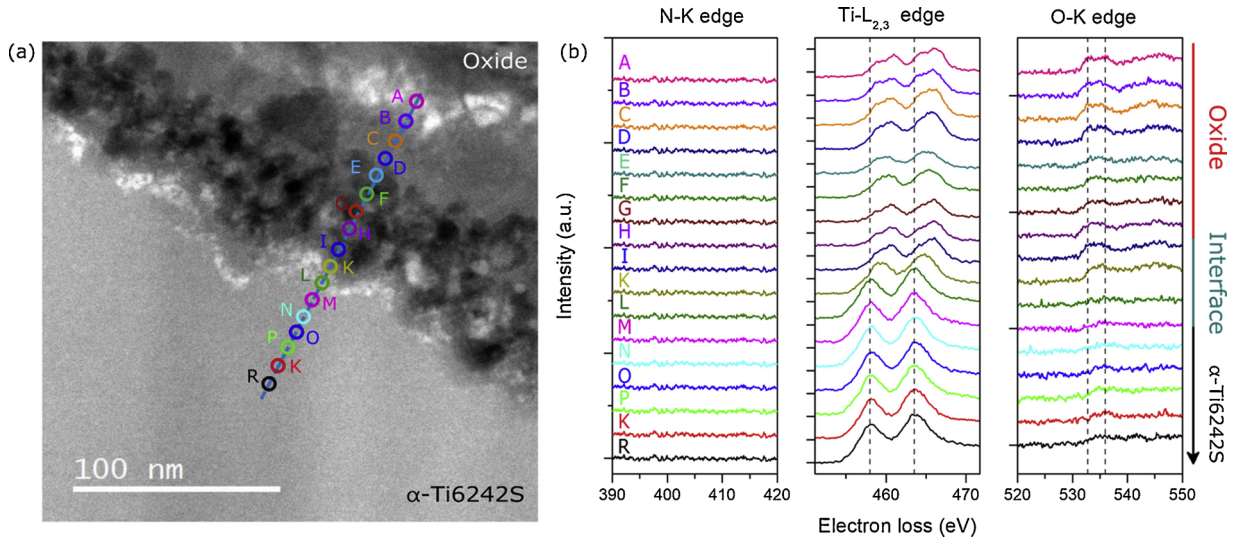


Fig. 8. STEM-HAADF image of region (II) of the Ti6242S oxidized in synthetic air of (a) the oxide-alloy interface and (b) its corresponding ELNES spectra of N-K, Ti- $L_{2,3}$ and O-K edges in each zone.

present in the TiN crystal structure. In our study and according to the Ti- $L_{2,3}$ energy shift, the nitride region can be divided into three parts. From the oxide layer towards Ti6242S alloy, the nitrogen concentration decreases from TiN (4 nm), few nanometers of $TiN_{0.5 < x < 1}$ to Ti_2N (11 nm) and then a nitrogen-rich α -phase within the alloy. The shift to lower energy value in the Ti- $L_{2,3}$ edge from TiN to Ti_2N was reported in Terada et al. as being equal to ~ 1 eV [8]. The increase in nitrogen vacancy closer to the alloy would increase the valence charge of Ti that leads to a decrease in L_3 DOS of Ti. N-K edge of TiN also exhibits a shift to lower energy loss value compared to N-K edge of N enriched Ti as present in the inset of Fig. 6b. Our results are in good agreement with the work of Terada et al. [8] for both Ti and N energy shifts to lower and higher energy loss values, respectively when nitrogen vacancy increases from TiN to Ti(N).

3.2. Sample oxidized in synthetic air: (Region II)

A second TEM FIB sample was extracted from a different region of the Ti6242S oxidized in synthetic air at 650 °C for 1000 h. In this

region, similar analysis was performed on a low magnification STEM-HAADF micrograph where the overall morphology (Fig. 7a) is almost identical to that of Fig. 1a. The oxide scale also measures $2 \pm 0.1 \mu m$ in thickness and porosity and stratification are present in the upper region of the oxide scale. The latter is also identified as rutile TiO_2 by SAED acquired in similar conditions as in region I. Qualitative EDX maps of the four chemical elements shown in Fig. 7b are similar to Fig. 1b. However, in this sample, EELS spectra show no detection of nitrogen in the oxide-alloy interface. For this, different positions of EELS spectra along a line profile are represented on the STEM image (Fig. 8a). In Fig. 8b, the spectra are divided into three parts: oxide, interface and Ti6242S regions. A decrease in oxygen intensity peak passing from Ti-rich oxide spectrum (A) to a slight oxygen detection in the alloy at spectrum (R) can be noticed. Ti- $L_{2,3}$ and O-K edges (Spectrum (A)) doesn't resemble to a rutile or anatase- TiO_2 where the asymmetry of the four peaks is different from the rutile TiO_2 presented in Region I or to literature data of anatase. Stoyanov et al investigated the lattice distortion accompanied with oxygen vacancies in seven kinds of Ti oxides from tetragonal rutile TiO_2 to cubic TiO structure [28]. They also

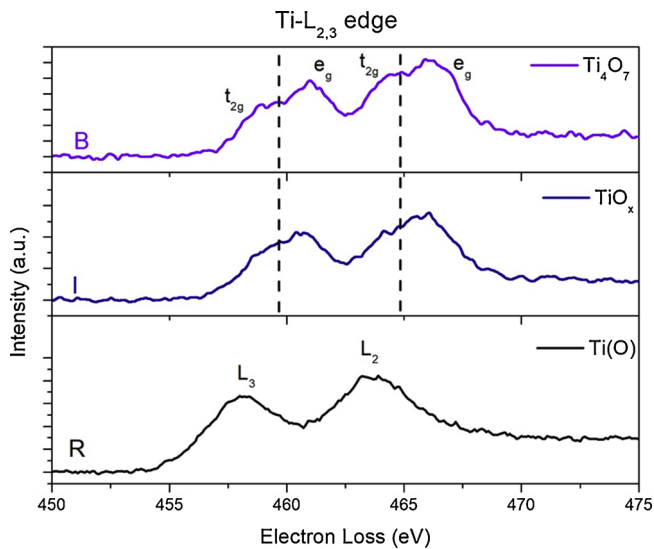


Fig. 9. Ti-L_{2,3} electron energy loss spectra (B), (I) and (R) taken from region (II) of the Ti6242S oxidized in synthetic air. The L₂ and L₃ peaks splits into four peaks as oxidation state increases.

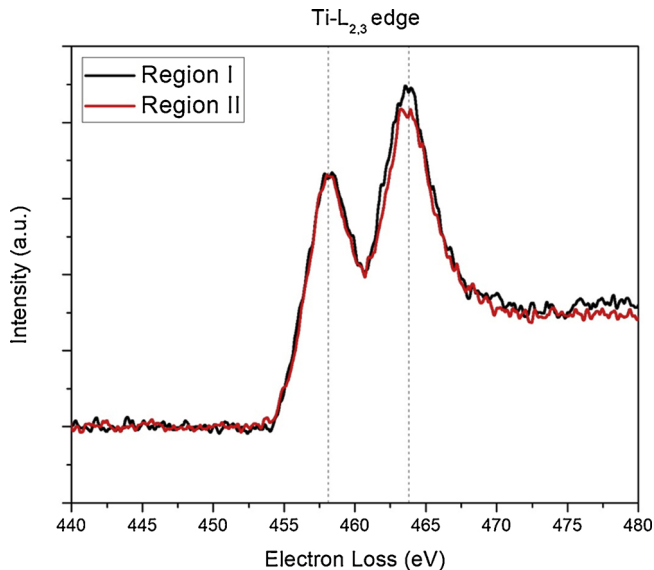


Fig. 10. Superposition of the Ti-L_{2,3} edge peaks in α -Ti6242S alloy for the sample oxidized in synthetic air for regions I and II.

monitored that the energy position of the Ti-L_{2,3} edges shift to lower energy when the oxidation state decreases. The major difference in the electron structure of different oxides such as TiO, Ti₂O₃ and TiO₂ is the degree of occupancy of the 2t_{2g} level where TiO has two electrons, Ti₂O₃ has one and none for TiO₂. In rutile/anatase, the energy position of Ti-L_{2,3} edge shifts to higher energy compared to Ti because there is no electron on the first unoccupied 2t_{2g} level where the screening is poorest. As the oxidation state decreases, the screening is better and the energy position of Ti-L_{2,3} edge is closer to metallic Ti. The fine structure of Ti-L_{2,3} and O-K edges of spectrum (A) was compared to the different oxidation states of Ti oxides presented in the work of Stoyanov et al. [28] and was identified as Ti₄O₇. Along the oxide-alloy interface, the fine structure of Ti-L_{2,3} edge exhibiting four peaks corresponding to Ti₄O₇ progressively changes to only exhibits two peaks for Ti. At the interface, without nitrogen detected, the shift in energy position of Ti-L_{2,3} edge to lower energy values indicates the decrease in oxidation state.

A comparison between spectra (B), (I) and (R), shows that at lower

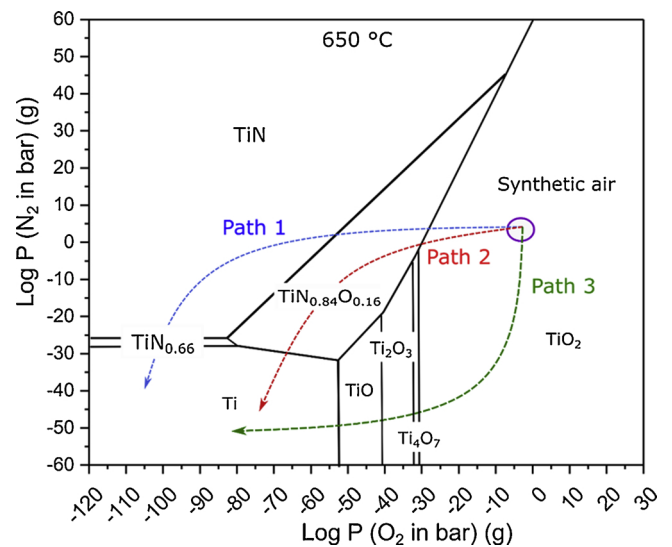


Fig. 11. Ti-N-O phase diagram at 650 °C.

oxidation states, L₃ and L₂ split to four peaks (Fig. 9). The decrease in oxidation state from Ti₄O₇ to TiO_x (x < 1.7) and to a solid solution of Ti (O) is then attributed to an increase in valence charge of Ti atoms and consequently a decrease in its binding energy. Therefore, a shift to lower energy loss value in EELS spectra is observed.

It is also worth noting that Ti-L_{2,3} edges acquired in the α -Ti6242S after the oxide-alloy interface in both regions are identical as shown in Fig. 10. This means that the solubility of oxygen or nitrogen in small quantities does not strongly affect the chemical nature of Ti in α -Ti6242S. Also, it is worth noting that neither oxygen nor nitrogen was detected by EELS in a TEM lamella extracted 300 μ m underneath the oxide layer of the sample oxidized in synthetic air for 1000 h at 650 °C (the data are not presented in this article).

Both observations of Ti6242S oxidized in synthetic air at 650 °C for 1000 h can be explained thanks to Ti-O-N phase diagram generated at 650 °C using HSC software [29], presented in Fig. 11 for an oxidation environment made in synthetic air. There exist few diffusion paths to reach titanium. One can cross the oxynitride, TiN and Ti₂N (path 1), as observed in region I, where another one can reach titanium right after the oxynitride (path 2). Another possible diffusion path would only cross oxides (path 3), like region II.

EELS spectra taken in region II of Ti6242S oxidized in synthetic air confirm 'path 3' with the decrease in oxidation states of Ti oxide as oxygen partial pressure decreases. On the other hand, formation of oxynitride/nitride layer confirms 'path 1' at low oxygen partial pressure plus at the interface of TiO₂. At high nitrogen partial pressure, inclusion of nitrogen atoms starts to fill the oxygen vacancies and oxynitrides are formed. Formation of oxynitride/nitride could act as a diffusion barrier for oxygen. Therefore, EELS spectra of region I confirm the previous hypothesis.

3.3. Sample oxidized in 80% Ar- 20% O₂ atmosphere

Same analysis as the two previous samples was performed on Ti6242S oxidized in 80% Ar- 20% O₂ atmosphere. The oxide scale of this sample is 10 μ m thick (Fig. 12a), five times thicker than that of the sample oxidized in synthetic air. The difference in oxide scale is indeed relevant to the oxidizing environment. A selected region of the FIB TEM sample is represented by STEM-HAADF image at the interface region (Fig. 12b). The STEM image shows clearly a difference in contrast from the alloy (light gray) to the oxide layer (dark gray). To identify the bright contrast in the STEM image, an EDX line scan is drawn to show qualitatively the chemical element variation at the oxide-alloy interface. Fig. 13 shows the intensity of the detected elements as a function

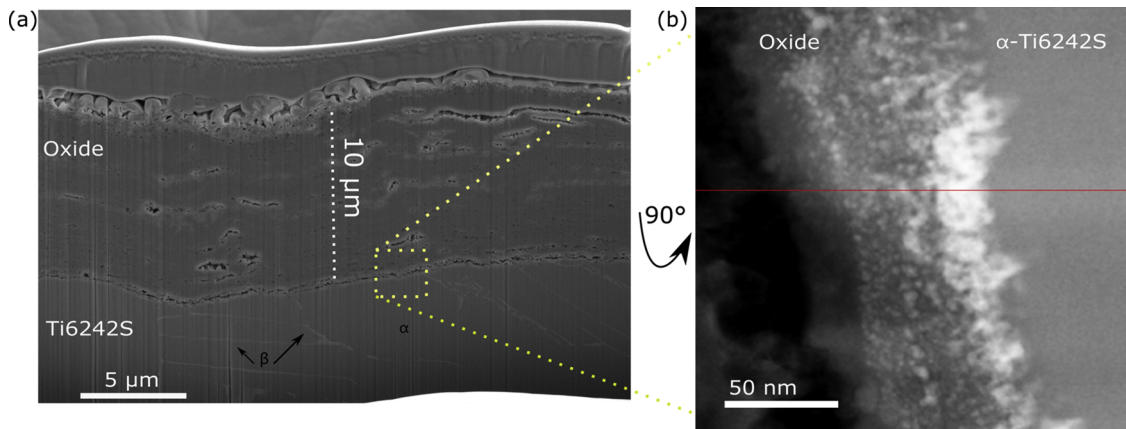


Fig. 12. (a) FIB SE image of Ti6242S oxidized in 80% Ar- 20% O₂ and (b) STEM-HAADF image of the selected area in (a) showing the oxide-alloy interface.

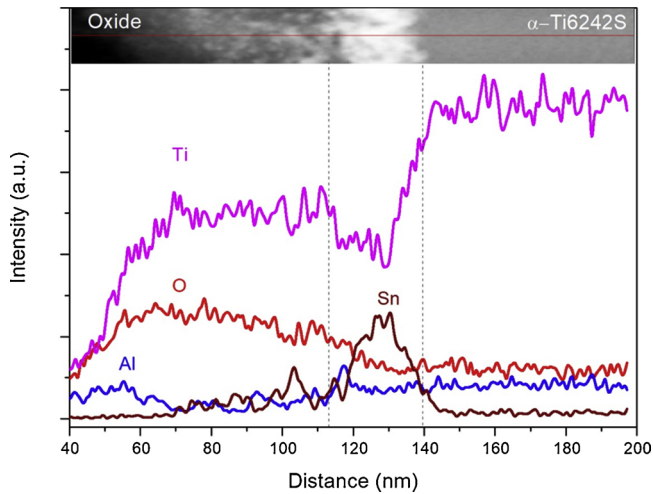


Fig. 13. EDX line scan across the oxide-alloy interface showing qualitatively the present chemical elements: Ti, Sn, and O elements.

of the measured distance. Starting from the oxide region on the left, apart from Ti and O elements, we notice the inclusion of Al for few nanometers in the oxide layer. Afterwards, on the bright region, the intensity of Sn increases along with a decrease in Ti and O intensities. This region corresponds to the oxide-alloy interface. Reaching the alloy,

Table 1

Comparison of the Ti-L₃ energy position of Ti6242S oxidized in 80%Ar-20% O₂ atmosphere.

Spectrum	Ti-L ₃ edge peak position (eV)	
A	a: 459	b: 461.1
B	460.9	
C	460.1	
D	459.4	
E	459	
F	458.5	
G	458.3	

Ti has the highest intensity counts compared with the presence of Al and O chemical elements that reflects the α -phase of Ti6242S.

In order to better study the chemical nature of this sample, EELS line scan is performed along the oxide-alloy interface on the STEM-HAADF image (Fig. 14a). Fig. 14b presents selected spectra of Ti-L_{2,3} and O-K edges.

Similar to the sample oxidized in synthetic air (region II), where no nitrogen is detected, O-K edge decreases in intensity as oxygen concentration is reduced passing from oxide to the alloy region. Ti-L_{2,3} edge of spectrum (A) is identified as Ti₅O₉ after comparing its fine structure with Stoyanov et al. along with O-K edge composed of two peaks at 532.5 and 535 eV. The O-K edge for spectra (B) and (C) decreases in intensity along with a change of the fine structure and a small shift to higher energy values. This is accompanied with a small shift of

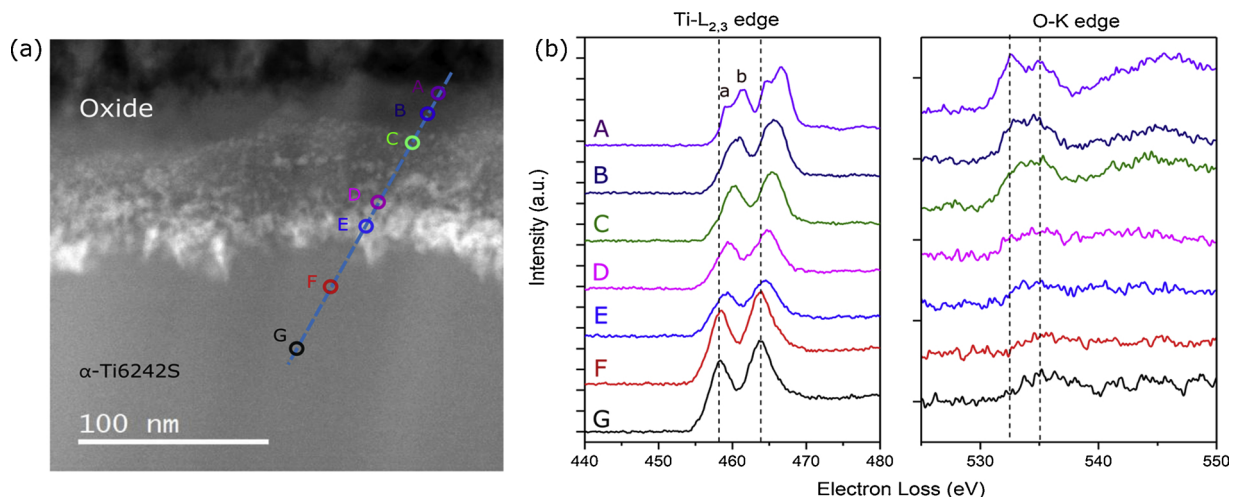


Fig. 14. STEM-HAADF image of the sample oxidized in 80%Ar-20% O₂ of (a) the oxide-alloy interface and (b) its corresponding ELNES spectra of N-K, Ti-L_{2,3} and O-K edges in each zone.

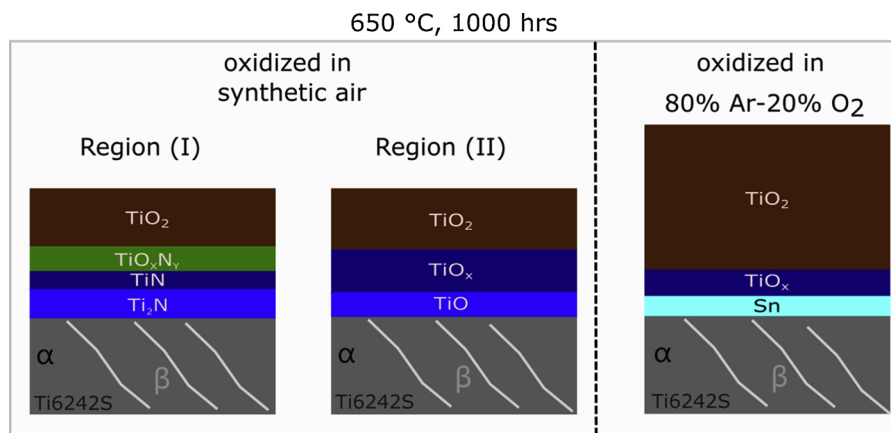


Fig. 15. Graphical representation of the observed microstructure changes in the three analyzed TEM samples.

Ti-L_{2,3} edge towards lower energy losses indicating a decrease in oxidation state. Closer to the interface, less oxygen concentration is detected as shown in the O-K edge of spectrum (D). At the interface, where Sn is segregated, the identified Ti-L_{2,3} edge intensity decrease at spectrum (E) is noticed. This is due to the diffusion of Sn identified as well by EDX. The shift of the Ti-L₃ edge peaks (between 458 and 461 eV) from spectrum (A) to (G) is summarized in Table 1. Indeed the values of Ti-L₃ edge are slightly higher than Stoyanov et al. by less than 1 eV [28]. This might be because the titanium oxide grew on top of the Ti6242S alloy oxidized at high temperature. The oxygen dissolution deep in the alloy was detected by EELS spectra, where oxygen dissolution is present after few hundreds of nm.

As a summary, the microstructure of the observed lamellas characterized by EELS is presented in Fig. 15. It has been observed that in the nitrogen-rich atmosphere, the two samples present different behaviors at the oxide-alloy interface keeping the same oxide scale. After oxidation in synthetic air, the nitride region is discontinuous along the oxide-alloy interface coupled with the decrease in the oxidation state of the titanium oxide. In the nitrogen-free atmosphere, nitrogen is not present at the interface whereas segregation of Sn is evidenced.

4. Conclusions

In this study, the oxide-alloy interface of Ti6242S alloy oxidized at 650 °C for 1000 h in both nitrogen free and synthetic air atmospheres was investigated by STEM-EELS technique:

- 1 EDX qualitative analysis showed a nitrogen enrichment at the oxide-alloy interface of the sample oxidized in synthetic air. Then the EELS technique allowed the identification of the phases present along the interface, based on the fingerprint approach using the fine structure and the shift in ELNES peak positions. Below the oxide scale, a 13 nm thick oxynitride was detected above a 30 nm zone composed of TiN and Ti₂N. Finally, a Ti(N) solid solution was observed underneath the nitrides. Thus, EELS technique has put in evidence its powerful detection of light elements in the excited atoms at a nanometer scale.
- 2 The observation of a second lamella extracted from the same sample (oxidized under synthetic air) revealed a different composition along the oxide-alloy interface. No nitrogen was detected which could be attributed to its absence at the interface or at a too low nitrogen content, making its detection difficult.
- 3 A third lamella was extracted from Ti6242S oxidized in nitrogen free atmosphere (80% Ar- 20% O₂) for 1000 h at 650 °C. An oxide layer 5 times thicker than the one formed in synthetic air was observed. A Ti(O) solid solution and a discontinuous Sn segregation were detected at the oxide-alloy interface. To our knowledge, the

phenomenon of Sn segregation is the first to be observed and its presence might be due to the large titanium and aluminum consumption during oxidation which lead to a higher Sn concentration compared to other elements at the interface.

These observations bring evidences of the nitrogen effect on the oxygen dissolution within Ti6242S alloy, when oxidized at 650 °C for 1000 h. The formation of interfacial nitrides or N-rich α-Ti solid solution decreases the oxygen dissolution in the alloy and then limits its ingress in the bulk material.

Data availability

The raw/processed data required to reproduce these findings cannot be shared at this time as the data also forms part of an ongoing study.

Acknowledgments

Authors thank the 'Fondation de la Maison de la chimie' for the post-doctorate grant of Iman Abdallah. Authors thank as well the personnel from 'Centre characterization Raymond Castaing (UMS 3623)' Claudie Josse, Alessandro Pugliara and Teresa Hungria for TEM sample preparation by FIB and STEM-EELS experiments.

References

- [1] W.L. Finlay, J.A. Snyder, Effects of three interstitial solutes (nitrogen, oxygen, and carbon) on the mechanical properties of high-purity, alpha titanium, JOM 2 (1950) 277–286, <https://doi.org/10.1007/BF03399001>.
- [2] H. Fukai, H. Iizumi, K. Minakawa, C. Ouchi, The effects of the oxygen-enriched surface layer on mechanical properties of α + β type titanium alloys, ISIJ Int. 45 (2005) 133–141, <https://doi.org/10.2355/isijinternational.45.133>.
- [3] H.A. Wriedt, J.L. Murray, The N-Ti (nitrogen-titanium) system, Bull. Alloy Phase Diagrams 8 (1987) 378–388, <https://doi.org/10.1007/BF02869274>.
- [4] A.M. Chaze, C. Coddet, The role of nitrogen in the oxidation behaviour of titanium and some binary alloys, J. Less-Common Met. 124 (1986) 73–84, [https://doi.org/10.1016/0022-5088\(86\)90478-9](https://doi.org/10.1016/0022-5088(86)90478-9).
- [5] A. Kanjer, V. Optasanu, M.C. Marco de Lucas, O. Heintz, N. Geoffroy, M. François, P. Berger, T. Montesin, L. Lavisé, Improving the high temperature oxidation resistance of pure titanium by shot-peening treatments, Surf. Coat. Technol. 343 (2018) 93–100, <https://doi.org/10.1016/j.surfcoat.2017.10.065>.
- [6] C. Dupressoire, A. Rouaix-Vande Put, P. Emile, C. Archambeau-Mirguet, R. Peraldi, D. Monceau, Effect of nitrogen on the kinetics of oxide scale growth and of oxygen dissolution in the Ti6242S titanium-based alloy, Oxid. Met. 87 (2017) 343–353, <https://doi.org/10.1007/s11085-017-9729-1>.
- [7] C. Dupressoire, M. Descoins, A. Vande Put, D. Mangelinck, P. Emile, D. Monceau, Understanding of the nitrogen effect on the oxidation behaviour of the Ti6242S titanium-based alloy- contribution of atom probe tomography, submitted to, Corros. Sci. (2019).
- [8] S. Terada, K. Asayama, M. Tsujimoto, H. Kurata, S. Isoda, Chemical shift of electron energy-loss near-edge structure on the nitrogen K-edge and titanium L3-edge at TiN/Ti interface, Microsc. Microanal. 15 (2009) 106–113, <https://doi.org/10.1017/S1431927609090175>.
- [9] Y. Kihn, C. Mirguet, L. Calmels, EELS studies of Ti-bearing materials and ab initio

- calculations, *J. Electron Spectros. Relat. Phenom.* 143 (2005) 117–127, <https://doi.org/10.1016/j.elspec.2004.02.170>.
- [10] C. Mirguet, L. Calmels, Y. Kihn, Electron energy loss spectra near structural defects in TiN and TiC, *Micron* 37 (2006) 442–448, <https://doi.org/10.1016/j.micron.2005.11.012>.
- [11] R.N. Shenoy, J. Unnam, R.K. Clark, Oxidation and embrittlement of Ti-6Al-2Sn-4Zr-2Mo alloy, *Oxid. Met.* 26 (1986) 105–124, <https://doi.org/10.1007/BF00664276>.
- [12] B. Sefer, Oxidation and Alpha-Case Phenomena in Titanium Alloys Used in Aerospace Industry: Ti-6Al-2Sn-4Zr-2Mo and Ti-6Al-4V (Licentiate dissertation). Retrieved from, (2014) <http://urn.kb.se/resolve?urn=urn:nbn:se:ltu:diva-26035>.
- [13] C. Beranger, G. et Coddet, Oxydation des métaux à haute température. Rôle des contraintes internes, *J. Microsc. Spectrosc. Électron.* 5 (1980) 793–814.
- [14] G. Bertrand, K. Jarraya, J.M. Chaix, Morphology of oxide scales formed on titanium, *Oxid. Met.* 21 (1984) 1–19, <https://doi.org/10.1007/BF00659464>.
- [15] J. Stringer, The oxidation of titanium in oxygen at high temperatures, *Acta Metall.* 8 (1960) 758–766, [https://doi.org/10.1016/0001-6160\(60\)90170-X](https://doi.org/10.1016/0001-6160(60)90170-X).
- [16] A.M. Chaze, C. Coddet, Influence of aluminium on the oxidation of titanium between 550 and 750 °C, *J. Less-Common Met.* 157 (1990) 55–70, [https://doi.org/10.1016/0022-5088\(90\)90406-A](https://doi.org/10.1016/0022-5088(90)90406-A).
- [17] J. Rakowski, D. Monceau, F.S. Pettit, G.H. Meier, R.A. Perkins, The oxidation and embrittlement of $\alpha 2$ (Ti3Al) titanium aluminides, *Maney Publ. IOM3, Inst. Mater. Miner. Min.* 2 (1993) 476–487.
- [18] A. Casadebaigt, J. Hugues, D. Monceau, Influence of microstructure and surface roughness on oxidation kinetics at 500–600 °C of Ti-6Al-4V alloy fabricated by additive manufacturing, *Oxid. Met.* 90 (5-6) (2018) 633–648, <https://doi.org/10.1007/s11085-018-9859-0>.
- [19] P.E.T. Ngnekou, M.C. Lafont, F. Senocq, L. Laffont, B. Viguier, J. Lacaze, Structural characterization of the scale formed on a Ti-46Al-8Nb alloy oxidised in air at 700 °C, *Intermetallics* 18 (2010) 226–232, <https://doi.org/10.1016/j.intermet.2009.07.013>.
- [20] R.F. Egerton, *EELS in the Electron Microscope*, Plenum, New York, 1986, <https://doi.org/10.1007/978-1-4419-9583-4>.
- [21] R.D. Leapman, L.A. Grunes, P.L. Fejes, Study of the L23 edges in the 3d transition metals and their oxides by electron-energy-loss spectroscopy with comparisons to theory, *Phys. Rev. B* 26 (1982) 614–635, <https://doi.org/10.1103/PhysRevB.26.614>.
- [22] P.L. Potapov, D. Schryvers, Measuring the absolute position of EELS ionisation edges in a TEM, *Ultramicroscopy* 99 (2004) 73–85, [https://doi.org/10.1016/S0304-3991\(03\)00185-2](https://doi.org/10.1016/S0304-3991(03)00185-2).
- [23] R. Brydson, H. Sauer, W. Engel, J.M. Thomas, E. Zeitler, N. Kosugi, H. Kuroda, Electron energy loss and X-ray absorption spectroscopy of rutile and anatase: a test of structural sensitivity, *J. Phys. Condens. Matter* 1 (1989) 797.
- [24] A. Gloter, C. Ewels, P. Umek, D. Arcon, C. Colliex, Electronic structure of titania-based nanotubes investigated by EELS spectroscopy, *Phys. Rev. B – Condens. Matter Mater. Phys.* 80 (2009) 1–6, <https://doi.org/10.1103/PhysRevB.80.035413>.
- [25] R. Brydson, B.G. Williams, W. Engel, H. Sauer, E. Zeitler, J.M. Thomas, Electron energy-loss spectroscopy (EELS) and the electronic structure of titanium dioxide, *Solid State Commun.* 64 (1987) 609–612, [https://doi.org/10.1016/0038-1098\(87\)90792-7](https://doi.org/10.1016/0038-1098(87)90792-7).
- [26] R. Ruus, A. Kikas, A. Saar, A. Ausmees, E. Nõmmiste, J. Aarik, A. Aidla, T. Uustare, I. Martinson, Ti 2p and O 1s X-ray absorption of TiO₂ polymorphs, *Solid State Commun.* 104 (1997) 199–203, [https://doi.org/10.1016/S0038-1098\(97\)00300-1](https://doi.org/10.1016/S0038-1098(97)00300-1).
- [27] D.W. Fischer, Molecular-orbital interpretation of the soft x-ray LII, III emission and absorption spectra from some titanium and vanadium compounds, *J. Appl. Phys.* 41 (1970) 3561–3569, <https://doi.org/10.1063/1.1659472>.
- [28] E. Stoyanov, F. Langenhorst, G. Steinle-Neumann, The effect of valence state and site geometry on Ti L3,2 and O K electron energy-loss spectra of Ti_xO_y phases, *Am. Mineral.* 92 (2007) 577–586, <https://doi.org/10.2138/am.2007.2344>.
- [29] A. Roine, *HSC Chemistry 7.0*, Outotec, (2009) www.outotec.com.